

UKAEA-CCFE-PR(18)40

M Cecconello, W Boeglin, D. Keeling, S Conroy, I Klimek,
R V Perez and the MAST team

Discrepancy between estimated and measured fusion product rates on MAST using guiding- centre approximation

Enquiries about copyright and reproduction should in the first instance be addressed to the UKAEA Publications Officer, Culham Science Centre, Building K1/0/83 Abingdon, Oxfordshire, OX14 3DB, UK. The United Kingdom Atomic Energy Authority is the copyright holder.

Discrepancy between estimated and measured fusion product rates on MAST using guiding-centre approximation

M Cecconello,¹ W Boeglin,² D. Keeling,³ S Conroy,¹ I Klimek,¹ R V Perez²
and the MAST team³

¹Department of Physics and Astronomy, Uppsala University, SE-751 05 Uppsala, Sweden

²Department of Physics, Florida International University, 11200 SW, Miami, FL 33199, USA

*³United Kingdom Atomic Energy Authority, Culham Centre for Fusion Energy, Culham Science Centre,
Abingdon, Oxon, OX14 3DB, UK*

Discrepancy between estimated and measured fusion product rates on MAST using guiding-centre approximation

M Cecconello¹, W Boeglin², D. Keeling³, S Conroy¹, I Klimek¹, R V Perez²
& the MAST team³

¹ Department of Physics and Astronomy, Uppsala University, SE-751 05 Uppsala, Sweden

² Department of Physics, Florida International University, 11200 SW, Miami, FL 33199, USA

³ United Kingdom Atomic Energy Authority, Culham Centre for Fusion Energy, Culham Science Centre, Abingdon, Oxon, OX14 3DB, UK

E-mail: marco.cecconello@physics.uu.se

Abstract. Experimental evidence is presented of a discrepancy between the predicted and measured D-D fusion products rates on MAST. Both the neutron and proton production rates, measured independently with a neutron camera and charged fusion product detector array, are approximately 40 % lower than those predicted by TRANSP/NUBEAM codes. This deficit is scenario independent and can not be explained by uncertainties in the typical plasma parameters suspected for such discrepancies such as the electron temperature, the plasma effective charge and the injected neutral beam power. Instead, a possible explanation is an overestimate of the neutron emissivity due to the guiding center approximation used in NUBEAM to model the fast ion orbits.

1. Introduction

Recently, the discrepancy between predicted and estimated neutron rates on JET has been the focus of a detailed study [1]. The authors of this study used an absolutely calibrated fission chamber [2] for measuring the neutron rate in several different JET plasmas and the TRANSP/NUBEAM codes [3, 4] to predict its expected values. The main conclusions of this study were that: *i*) the measured neutron rate was smaller than the predicted one (the so-called neutron deficit) by a factor that ranged from 0 to 50 % depending on the plasma scenario; *ii*) no clear correlation between the uncertainties in the main plasma parameters input to TRANSP/NUBEAM and the neutron deficit could be found; and *iii*) that MHD activity was not the cause of this deficit. Possible causes for the observed neutron deficit suggested by the authors of that study included: unknown physical processes leading to large fast ion redistribution, calibration errors, uncertainties in the DD fusion reaction cross-sections and in the fast ions slowing down models used in NUBEAM.

In this work we report similar observations on the Mega Ampere Spherical Tokamak (MAST) [5]. In addition to finding a neutron deficit between measurements and TRANSP/NUBEAM prediction, we have measured a similar deficit also in the proton rates production. The measured neutron and proton production rates on MAST are smaller than the expected ones by a similar amount to the one found on JET, approximately 40 %. Contrary to the observation in JET though, the discrepancy in MAST is roughly the same for all investigated scenarios when anomalous transport of fast ions due to MHD instabilities is accounted for. In a spherical tokamak, large fast ion populations as those originating from neutral beam injection heating, are not only responsible for the vast majority of all fusion reactions (the thermal reactivity is typically less than 5 %), but they can excite MHD instabilities that cause their redistribution and loss. Fusion product diagnostics can therefore provide information on the confinement of fast ions and the comparison between predictions and measurements on an absolute scale is thus of paramount importance in understanding the underlying physics used in the modelling codes as well as in testing of the code themselves in reference scenarios, such as those where no or little fast ion redistribution is expected.

This work presents new experimental evidence for the discrepancy between predicted and measured fusion products rates when the guiding centre approximation is used to model the entire fast ions orbits, as is done in NUBEAM. A systematic study of the possible causes for such discrepancy, described in detail in this paper, has excluded all but one, namely the role of the fast ions full orbits in the fusion reactivity. Contrary to JET, the confining magnetic field in MAST is quite small resulting in fast ions with energies in the tens of keV to have large Larmor radii. This in addition with the small size of MAST plasmas compared to the fast ions Larmor radii combined with quite steep gradients in the plasma density and temperature has been found to have an effect on the neutron emissivity [6, 7]. Modelling of the fusion products rates with full gyro-orbit codes is outside the scope of this work but, as a result of the conclusions here reached, of extreme importance.

The paper is organized as follows. The database of MAST plasma scenarios and discharges and the fusion products diagnostics used in this study are presented in sections 2 and 3 respectively: in particular, section 3.1 describes the synthetic diagnostics used to estimate the expected fusion product rates starting from the neutron emissivity profiles calculated by TRANSP/NUBEAM. Section 4 is devoted to the comparison between measurements and predictions while the possible sources for the observed discrepancies are discussed in detail in section 5. Finally the conclusions are presented in section 6.

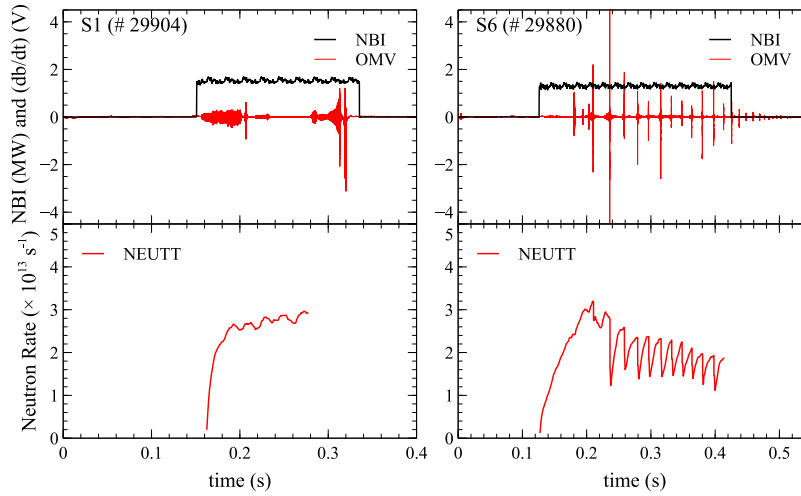


Figure 1 – Time traces of the NBI heating signal (black) and of a Mirnov pick-up coil (red) for a representative plasma discharge for two scenarios: quiescent plasma, left panels; saw-teething plasma, right panels. The neutron rate shown in the bottom panel is the predicted one from TRANSP/NUBEAM.

2. Plasma scenarios

MAST is a medium sized spherical tokamak with an aspect ratio $R/a \approx 0.85/0.65 \approx 1.3$ and capable of sustaining plasma discharges with plasma current in the range 0.4 to 1.0 MA and temperatures as high as 2 keV in a very low toroidal magnetic field (typical values are in the range 0.45 to 0.6 T). Two Neutral Beam Injectors (NBIs) provide additional heating (up to 3.5 MW) and are the main source of fast ions in MAST and the only source of neutron emission via the beam-thermal and beam-beam reactions up to a maximum neutron yield of about $Y \leq 2 \times 10^{14} \text{ s}^{-1}$. MAST is capable of a wide range of plasma scenarios with different divertor configurations such the up-down symmetric Double Null Divertor (DND) and the down-shifted Lower Single Null Divertor (LSND) scenarios, it can be operated in L and H-modes and the safety factor profile can be either monotonic or characterized by reversal in the core. MAST also exhibits a very rich set of MHD instabilities driven both by the background plasma equilibrium, such as the sawtooth instability and the edge localized modes, and by the presence of a large, super-Alfvénic fast ion population, such as Toroidal Alfvén Eigenmodes (TAEs), fish-Bones (FBs) and Long-Lived Modes (LLMs). The mechanism by which TAEs and FBs are excited is the free-energy made available by a NBI heating

Scenario	I_p (kA)	P_{NBI} (MW)	Y_{FC} ($\times 10^{13} \text{ s}^{-1}$)	Conf.	CFPD	Notes
S1	800	1.50	3.0	DND	Yes	Quiescent MHD
S2	800	1.50	5.6	DND	Yes	Intermediate MHD
S3	800	2.75	9.4	DND	No	TAEs, large FBs and LLMs
S4	1000	3.40	15.0	DND	No	TAEs, FBs and LLMs
S5	630	1.50	5.0	LSND	No	TAEs, FBs and LLMs
S6	560	1.30	2.0	DND	Yes	Sawtooth

Table 1 – Summary of the plasma scenarios exhibiting fusion product deficit. Neutron yield values indicate the maximum measured value by the fission chamber. Plasma configurations are Double Null Divertor (DND) and Lower Single Null Divertor (LSND). The Charged Fusion Product Detector (CFPD) was not available for all series.

Scenario	Pulse numbers
S1	29904 , 29905, 29906, 29908, 29909, 29910
S2	29222, 29917, 29924 , 29928, 29929, 29931
S3	29975, 29976 , 29980
S4	29132, 29181, 29207, 29208, 29209, 29210 , 29359
S5	27932, 27934, 27935, 27936, 27938
S6	29879, 29880 , 29881, 29882, 29884, 29885

Table 2 – List of plasma discharges used in this study. In bold, the representative plasma discharge for each scenario that has been modelled in TRANSP.

driven large fast ion pressure with a very steep spatial gradient. These instabilities are responsible for the redistribution and loss of fast ions and the consequent reduction in the neutron emissivity [8]. From a fast ion perspective, MAST plasma discharges can then be divided in “quiescent” scenarios characterized by no or very limited fast ion redistribution and in “non-quiescent” scenario where significant fast ion redistribution occurs. Table 1 summarizes the database of discharges used in this study which cover a wide range of plasma currents, from 0.5 to 1.0 MA, with different level of NBI heating, from 1.3 to 3.4 MW, in DND and LSND configurations grouped in six scenarios. Scenarios S_1 and S_6 are quiescent scenarios where little or no fast ion redistribution is occurring during parts of the discharge. In the case of scenario S_6 strong fast ion redistribution occur at the sawtooth crash but the fast ion population recovers fairly quickly so that in the inter-sawtooth crash period no redistribution is occurring. Scenarios S_2 to S_4 are characterized by different levels of fast ion redistribution. Scenario S_5 , which exhibits instabilities very similar to those of S_3 and S_4 , is included in the database to provide a historical perspective on the fusion products discrepancy as the discharges in S_5 were carried out almost two years before those of all the other scenarios. An example of the different nature and level of MHD activity in quiescent and non-quiescent scenarios is shown in figure 1 where the signal from a Mirnov pick-up coil is shown for selected discharges for scenarios S_1 and S_6 together with the time trace of the NBI power and the resulting simulated neutron rate. Thanks to MAST high reproducibility, all the discharges within each scenarios are almost identical: this has been exploited to measure the neutron emissivity profile as discussed in section 3. Table 2 list the discharges included in each scenario with those in bold being modelled with the codes TRANSP/NUBEAM (see section 3.1) as representative discharges for each scenario.

3. Fusion product diagnostics

The two principal diagnostics for this study are the Neutron Camera (NC) and the Charged Fusion Products Detector array (CFPD). A detailed description of these two diagnostics can be found in [9, 10].

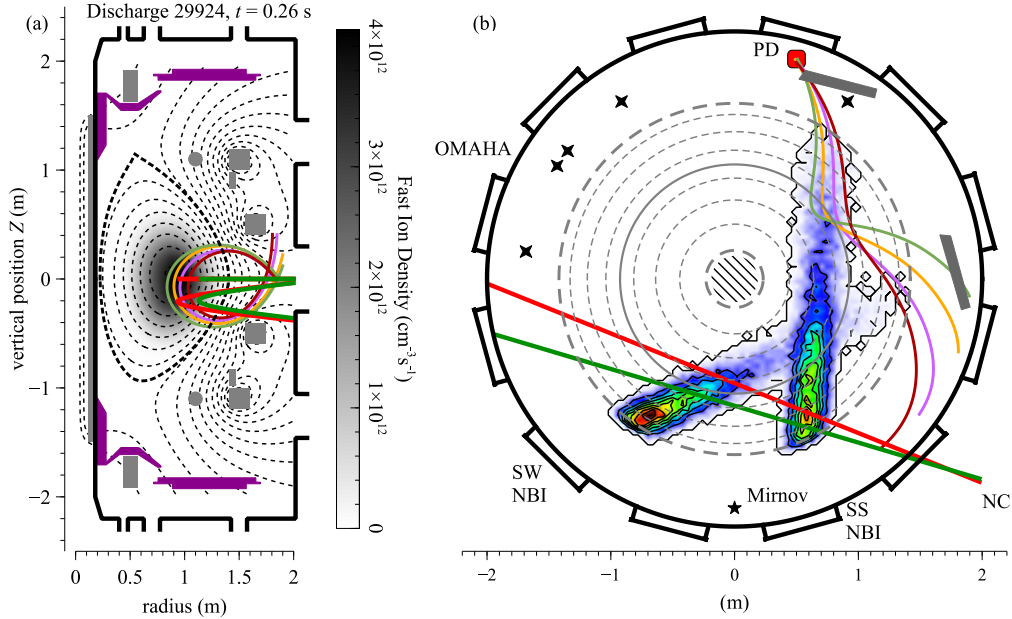


Figure 2 – Overview of the sight-lines looking at the plasma core for the neutron camera (red and green solid lines) and for the charged fusion products detector (pale green, yellow, magenta and brown) on a poloidal cross-section (a) and on the equatorial plane (b) together with the slowed down fast ion density shown in panel (a) and the fast ion birth location from the neutral beam injection in panel (b).

An overview of the plasma regions probed by the NC and the CFPD is shown in figure 2. The NC views the plasma along two collimated lines of sight on the equatorial plane through a thin stainless steel flange; two additional lines of sight look at the plasma 20 cm below mid-plane. The NC sightlines impact parameter p can be changed in between plasma discharges thus allowing the measurement of the neutron emissivity covering the entire plasma region from the inboard to the outboard side. The NC detectors consist of liquid scintillators (EJ-301 type) coupled to photo-multipliers. Each detector is equipped with a ^{22}Na source and connected to a LED source and both are used to correct for gain shifts in the PMT gain due to high count rates and the stray magnetic field. The light output of the EJ-301 scintillator to incident γ -rays and neutrons has been provided by the detector manufacturer. The efficiency of the detectors to 2.45 MeV neutrons from the DD fusion reaction has been determined by a combination of MCNP simulations [11] and absolute calibration of the acquisition energy threshold in MeV electron equivalent using multiple standard γ -ray sources. The results of such simulations agree with similar Monte Carlo simulations available in literature validated by measurements of the efficiency to mono-energetic neutron beams [12–16]. The efficiency so determined for the NC detectors is $\epsilon = 13\%$. The attenuation of the neutron flux through the thin stainless steel flange has also been estimated via MCNP simulations resulting in a transmission coefficient $\eta = 0.904$.

The CFPD consists of four Silicon Surface-Barrier (SBB) diodes mounted inside a shielding case with collimated views of the plasma and shielded against light and x-ray radiation by a $0.8\ \mu\text{m}$ thick aluminium foil. The active layer at $100\ \mu\text{m}$ thick is designed to fully stop the 3 MeV protons while being insensitive to neutrons. The CFPD is mounted on a linear manipulator arm which provides limited radial scan capabilities, from $R = 0.75\ \text{m}$ to $R = 1.05\ \text{m}$, along the mid-plane. An example of the typical trajectories of the 3 MeV protons from the DD reaction reaching the detectors, calculated for the specific magnetic equilibrium reconstructed with EFIT [17], are shown in figure 2. Two out of the four channels in the CFPD are partly shadowed by one of the NBI dumps as shown in figure 2: in this study therefore only results from the two channels not affected by the shadowing are presented. This non-optimal experimental set-up was due to the limited time available for the installation of the CFPD on MAST (only one port on the machine could be made available) and for carrying out these measurements before MAST went into

shutdown. The efficiency of the CFPD for 3 MeV protons is approximately $\epsilon_{\text{SBB}} = 97\%$. The efficiency of SSB with the proper minimum depletion depth is in general accepted to be 100 % for a properly working detector. Charged particle detection losses are mostly due to missed proton pulses due to either large electrical noise signals and pile-up events (e.g. pulses that are less than approximately 400 ns apart and are therefore not identified as two individual pulses). In order to determine such effect on the detection efficiency, artificial signals have been added to real data and analyzed: the number of simulated events losses at the measured particle rate has then been used as a measure of detection efficiency.

In addition to the NC and CFPD, MAST is equipped with an absolutely calibrated ^{235}U Fission Chamber (FC) used to monitor the global neutron yield Y_n with a time resolution of 10 μs [18]. The calibration of the FC was carried out once at the very beginning of MAST operations and its calibration has been tracked through the years with a neutron activation system.

3.1. Synthetic diagnostics

The NC and CFPD measure the Count Rate (CR) with which neutrons and protons are detected. In order to compare the measured CRs with theoretical predictions, synthetic diagnostics have been developed. The synthetic diagnostics combine the plasma equilibrium, the neutron emissivity $\epsilon_n(R, Z)$ on a poloidal cross-section calculated by TRANSP/NUBEAM with the geometry of the lines of sight and the detectors' response function (including their efficiency) to provide the expected neutron and proton count rates. A detailed description of the NC synthetic diagnostic can be found in [19]. The predicted NC count rate for a given impact parameter p , $\nu_n(p)$, is given by:

$$\nu_n(p) = \eta \epsilon \sum_{i,j} \epsilon_n(R_{i,j}, Z_{i,j}) \Omega(p; R_{i,j}, Z_{i,j}) \quad (1)$$

where $\Omega(p; R_{i,j}, Z_{i,j})$ is the 3D solid angle subtended by a volume element of the plasma, ϵ_n , at the NC detector viewing the plasma with tangency radius p . Summation is over all volume elements used in NUBEAM to estimate the neutron emissivity on a poloidal cross-section. The solid angle $\Omega(p; R_{i,j}, Z_{i,j})$ is calculated with a Monte Carlo code which implements the full 3D geometry of MAST and of the NC. The code has been validated against analytical calculations and good agreement has been found (relative difference less than 5 %). Already in a previous work [19] it was observed that the profile of the NC count rate as a function of the impact parameter $\nu_{\text{NC}}(p)$ was in good agreement with $\nu_n(p)$ only if the latter was multiplied by a constant scaling factor $k \approx 0.7$, that is $\nu_{\text{NC}}(p) = k\nu_n(p)$. A systematic validation of the neutron emissivity profile $\epsilon(R, Z)$ calculated by NUBEAM was then carried using the Directional RELativistic Spectrum Simulator (DRESS) code [20]. Good agreement was found between DRESS and NUBEAM neutron emissivities (relative difference less than 1 %). DRESS can model the energy spectra of the products from fusion reactions involving two reactants with arbitrary velocity distributions employing fully relativistic kinematic equations to calculate the energy of the fusion products. Input to DRESS are the equilibrium magnetic field and the reacting fuel ions velocity distribution function which in this validation was provided by NUBEAM itself.

The simulation of CFPD count rates is based on the same TRANSP/NUBEAM simulations used for the NC. In this case, the proton emissivity $\epsilon_p(R, Z)$ is assumed to be equal to the neutron one both in its spatial distribution and intensity and that protons do not undergo collisions between their birth and the detector. The probability for such a reaction along a path length of 400 m in a plasma density of $6 \times 10^{19} \text{ m}^{-3}$ has been estimated to be of the order of approximately 10^{-7} . The spatial distribution is identical since the fuel and fast ion spatial distribution is the same for both reaction channels. The intensity of the neutron and proton emissivities can be assumed identical since the ratio of the thermal emissivity varies between 1.02 and 1.03 in the ion temperature range of interest ($T_i < 1.0 \text{ keV}$) and the ratio of the beam-thermal cross-sections for the beam-target reactions $\text{D(d,n)}^3\text{He}$ and $\text{D(d,p)}\text{T}$ varies between 0.97 and 0.98 for the fuel ion and NBI energies of the plasma scenarios here studied [21]. Interpolation over the RZ plane is carried out to estimate the proton emissivity $\epsilon_p(R, Z)$ along the proton trajectories which are backward calculated with a full orbit following code in the equilibrium magnetic field calculated via EFIT. The full-orbits are backtracked starting from the CFPD position until they intersect the vessel walls, the coils and other obstacles: the path length of all simulated orbits has never exceeded 400 m in this analysis. For each detector-collimator pair a large number of orbits are calculated (between 81 and 6)

to take into account the non infinitesimal size of the field of view by dividing the collimator and detector areas in a 3×3 or 5×5 arrays. The expected CFPD count rates ν_p is then given by the integration of the proton emissivity along each orbit as:

$$\nu_p = \epsilon_{\text{SBB}} \sum_i A_i \int_{\ell_i} \varepsilon_p [R(\ell), Z(\ell)] d\ell \quad (2)$$

where ℓ is the position of the proton along its orbit, A_i is the phase space acceptance for this bundle and the summation is carried out over all the orbit bundles.

A standard output of TRANSP/NUBEAM is the total neutron yield Y_n which is usually compared with the one measured by an absolutely calibrated fission chamber, Y_{FC} . On MAST, for quiescent scenarios, good agreement is found between the two if Y_{FC} is multiplied by 0.9, a correction factor which accounts for drifts in the FC since its absolute calibration. In the case of non-quiescent scenarios, $Y_n > Y_{\text{FC}}$ an observation which is usually interpreted as a reduction in the fast ion confinement due to the energetic particle modes. Agreement between the two is recovered by introducing in TRANSP/NUBEAM an anomalous fast ion diffusion coefficient D_a to account for the redistribution of fast ions. The anomalous fast ion diffusion coefficient can be specified by the user in the input file to have an energy, space and time dependency which is typically adjusted so that the predicted and measured neutron yields match. On MAST, good agreement can be obtained between the predicted and measured neutron yields using a D_a which is constant in space and energy and varies only in time: typical values for D_a ranging from $0 \text{ m}^2\text{s}^{-1}$ for quiescent scenarios up to $3 \text{ m}^2\text{s}^{-1}$ for non-quiescent scenarios.

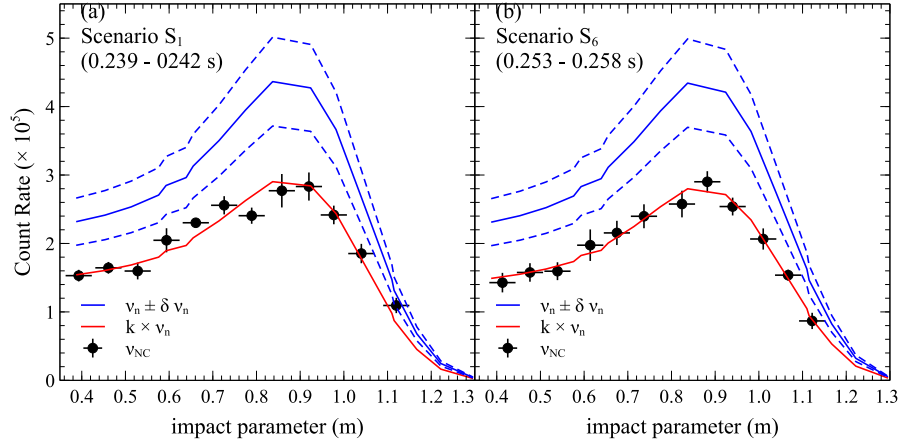


Figure 3 – Comparison between measured (solid circles) and predicted (continuous lines) neutron camera count rates for scenario S_1 and S_6 in panels (a) and (b) respectively in selected time intervals. Predicted count rates CR_{TR} (solid blue line) are shown with their uncertainties (dashed blue lines) and multiplied by the scaling factor k (red lines): in this case, $\bar{k} = 0.665$ (panel (a)) and $\bar{k} = 0.645$ (panel (b)).

The neutron emissivity used in equation (1) is calculated by NUBEAM as a non flux-surface averaged quantity in contrast to standard output which is flux-surface averaged. In order for the neutron emissivity to be calculated with low statistical variance, each TRANSP/NUBEAM simulation discussed in this work has been carried out with a large number of Monte Carlo model particles (5×10^4) representing the NBI fast ions, resulting in long computational times. The implication of this will be discussed more in detail in section 4.2. As for the total neutron yield, good agreement between Y_n and Y_{FC} is achieved even when a low number of Monte Carlo model particles (10^3) is used in the TRANSP/NUBEAM modelling. For example, the standard deviation in the relative difference of Y_n between simulations with 10^3 and 5×10^4 particles is approximately 0.025 but the required simulation time for the former is approximately 30 times shorter.

4. Simulations versus observations: a systematic study

In this section, the evidence of a systematic discrepancy between predicted and measured count rates for the fusion products is presented. Predicted 2.45 MeV neutron and 3 MeV proton count rates have been estimated from TRANSP/NUBEAM simulations with large number of Monte Carlo particles at selected times during the plasma discharge for all representative pulses listed in table 2. The neutron emissivity at these selected times is the average over a 3 ms time interval for the NC and between 5 and 20 ms for the CFPD. The quiescent scenarios, discussed in section 4.1, are characterized by little or no fast ion redistribution and therefore have been simulated setting $D_a = 0 \text{ m}^2\text{s}^{-1}$. The fusion product discrepancy was also found in a wider range of plasma scenarios characterized by non-quiescent MHD activity. These scenarios were simulated first with no anomalous fast ion diffusion and then by adjusting D_a to match the neutron yield measured by the FC as discussed in detail in section 4.2.

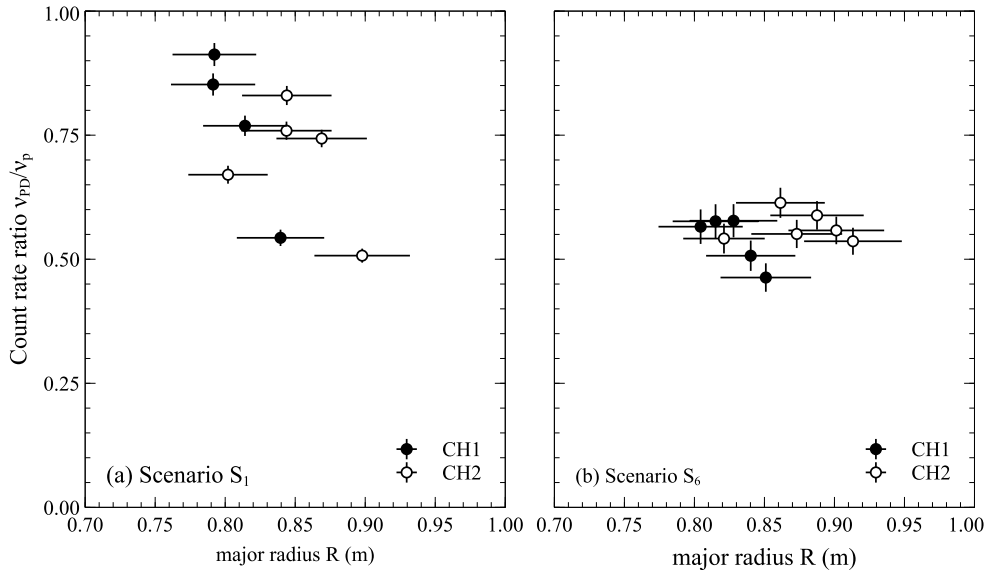


Figure 4 – Ratios between the charged fusion product detector count rates of the proton emission CR_{PD} measured by two channels to those predicted by TRANSP CR_{TR} for four plasma discharges of scenario S_1 for $t \approx 0.21 \text{ s}$ in panel (a) and for five plasma discharges of scenario S_6 in panel (b) for $t \approx 0.25 \text{ s}$, before a sawtooth crash. The horizontal bars indicate the range of mid-plane radii covered by each CFPD detector channel

4.1. Quiescent MHD scenarios

Figure 3 shows two typical examples of the discrepancy observed between predicted neutron count rates ν_n and those measured by the neutron camera, ν_{NC} . The profile $\nu_{\text{NC}}(p)$ is obtained by combining all the plasma discharges for each scenario while the predicted profile $\nu_n(p)$ is based on the TRANSP/NUBEAM modelling of plasma discharges #29904 and #29880. The results presented in figure 3 highlight the fact that TRANSP/NUBEAM simulations are able to correctly reproduce the shape of the neutron camera count rate profile but not its amplitude. Good agreement between predicted and measured count rates is recovered if ν_n is multiplied by a factor $\bar{k} = 0.67 \pm 0.02$ for S_1 and $\bar{k} = 0.65 \pm 0.02$ for S_2 . The quantity \bar{k} is the average of the ratios $k(p_i) = \nu_{\text{NC}}(p_i)/\nu_n(p_i)$. This discrepancy can not be explained even when taking into account the uncertainties in the input parameters to TRANSP/NUBEAM. The plasma parameters that affect the neutron emissivity are the electron temperature T_e and the effective charge Z_{eff} while the electron density n_e and the ion temperature T_i have a negligible effect [19]. When a relative uncertainty of 10 % is included in both T_e and Z_{eff} (typical values on MAST) the discrepancy between ν_{NC} and ν_n is still larger than the error bars for both scenarios as shown in figure 3 by the dashed lines. In order

to match ν_n to ν_{NC} it would be necessary to either double the value of the core Z_{eff} (from 1.5 to 3.1) or reduce the electron temperature by approximately 26 %. In both cases, these are variations much larger than those that are deemed acceptable given their uncertainties: the relative uncertainty on the electron temperature has been determined to be less than 5 % [22] and less than 30 % for Z_{eff} [23]. Additional TRANSP/NUBEAM simulations have been performed where the NBI energy and densities were changed. In such case, in order to reproduce the experimental results the NBI energy should be reduced from 60 to 52.5 keV or the beam density by 35 %. These large variations are also beyond their accepted uncertainties and are therefore not credible [24]. As a final comment on the neutron count rates, it is worth nothing that the predicted count rates are based only on the contribution of uncollided neutrons, that is neutrons that are emitted from the plasma and reach the detector without making any collision. A fraction of the measured count rates, however, is due to collided neutrons since the detectors can not discriminate between uncollided and collided neutrons. The fraction of scattered neutrons has been estimated to be less than 10 % for impact parameters $p \leq 1.1$ m [9]. As a result, the actual ratio \bar{k} would be reduced by a similar amount giving $k \approx 0.59$ indicating an even larger discrepancy between experiment and model.

A similar discrepancy is observed for the CFPD count rates of the 3 MeV protons ν_{PD} as shown in figure 4. The profile of the ratio ν_{PD}/ν_p is shown for selected time intervals for both S_1 and S_6 : in this case we observe $\bar{k} = 0.72 \pm 0.02$ and $\bar{k} = 0.57 \pm 0.01$. It is worth mentioning that in the case of S_6 , the deficits in ν_{NC} and ν_{PD} are not affected by the sawtooth crashes, i.e. the deficit is approximately the same as that indicated when measured before and a few ms after each sawtooth crash (the neutron rate is averaged in 3 ms time intervals, while the proton rate in 5 ms time intervals).

Finally figure 5 shows the scaling between TRANSP/NUBEAM predictions and measured count rates for each pulse, time and impact parameter (for the NC) and radial position (for the CFPD). As can be seen, most the experimental measurements are characterized by a deficit between 0 and 50 % with an average value of $k = 0.64 \pm 0.02$ and 0.62 ± 0.09 for the NC and the CFPD respectively. A few NC data points for scenario S_1 fall on the 100 % line: these data points all come from measurements at large impact parameter $p \gtrsim 1.1$ m. The reason for this deviation from the overall trend is not clear but it might be due to the peculiarity of this scenario since such deviations are not observed in all other scenarios for similar impact parameters.

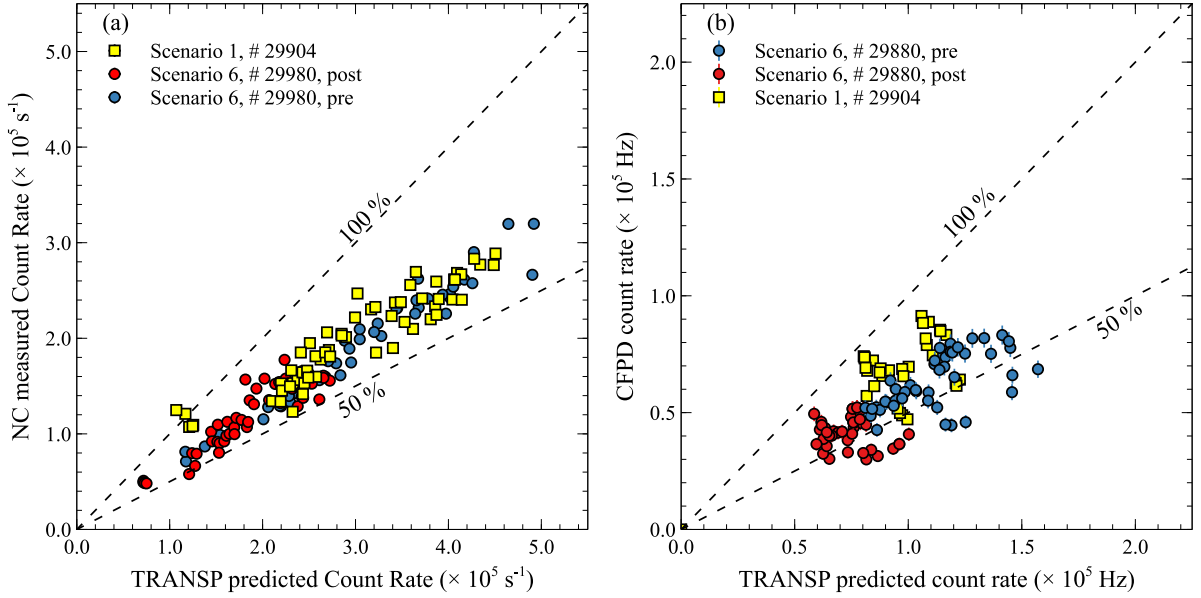


Figure 5 – Comparison between TRANSP predicted and measured count rates by the neutron camera (panel (a)) and the charged fusion product detectors (panel (b)) for scenarios S_1 and S_6 . TRANSP predictions with no anomalous fast ion diffusion coefficient. Each experimental data point represent the ratio between individual NC/CFPD channels and the TRANSP predicted CRs for selected times during the plasma discharge. The labels “pre” and “post” refers to the time intervals before and after a sawtooth crash.

4.2. Non-quiet scenarios

The comparison between the predicted and measured count rates ν_n and ν_{NC} is carried out firstly by setting $D_a = 0 \text{ m}^2\text{s}^{-1}$ even if fast ion redistribution and the associated reduction in the neutron emissivity is expected. The rationale for this is to see by how much TAEs, FBs and LLMs affect the scaling factor k thus providing an estimate of the redistribution of fast ions based only on the neutron camera measurements. An example of this comparison is shown in panels (a) and (b) of figure 6 for scenarios S_3 and S_4 respectively. For the time intervals indicated, the scaling factor is $\bar{k}_a = 0.47$ and $\bar{k}_a = 0.39$ respectively, where the index “a” indicate that this scaling factor applies in the presence of anomalous fast ion redistribution: as expected we observe that $k > k_a$. Note that in these scenarios too, the simulated count rate profile well matches the shape of the experimentally measured one. The dependency of \bar{k}_a on

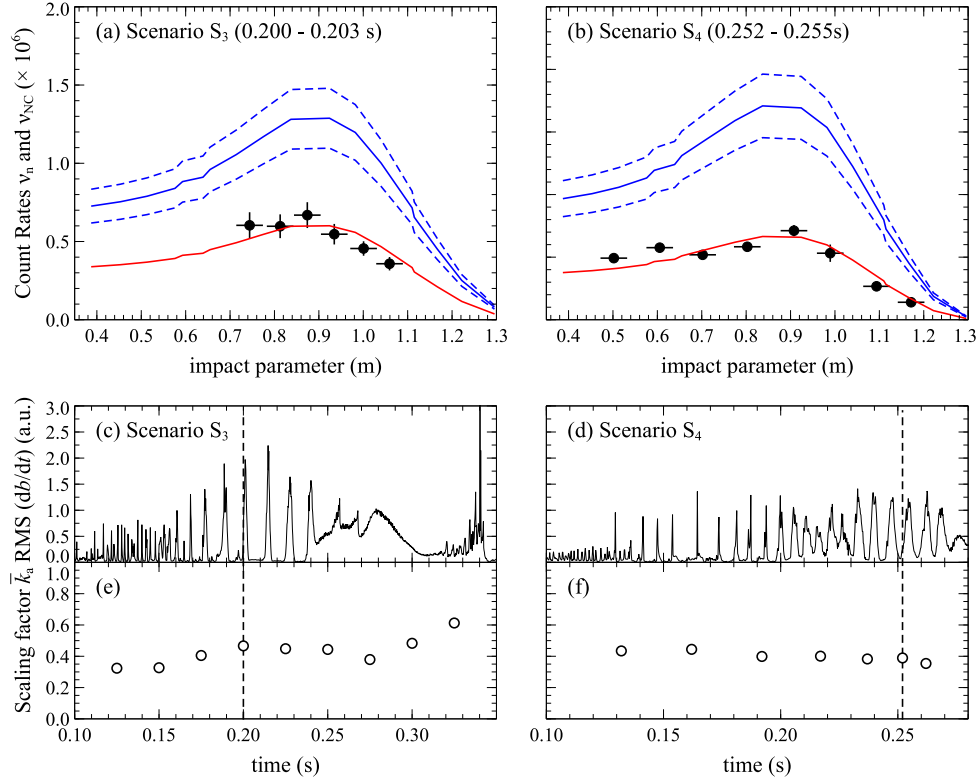


Figure 6 – Comparison between measured (solid circles) and predicted (continuous lines) neutron camera count rates for scenario S_3 and S_4 in panels (a) and (b) respectively. Predicted count rates CR_{TR} (solid blue line) are shown with their uncertainties (dashed blue lines) and multiplied by the averaged anomalous scaling factor \bar{k}_a (red lines): $\bar{k}_a = 0.466$ (panel (a)) and $\bar{k}_a = 0.389$ (panel (b)). The time evolution of the RMS of the Mirnov coil signals is shown in panels (c) and (d) for scenarios S_3 (# 29976) and S_4 (# 29210) respectively. Panels (e) and (f) show the corresponding evolution of the averaged anomalous scaling factor \bar{k}_a . The vertical dashed lines indicate the times of the count rate profiles shown in panels (a) and (b).

the MHD activity is shown in panels (c) to (f) of figure 6 where the evolution in time of the RMS of the signal of a Mirnov pick-up coil is plotted together with $\bar{k}_a(t)$ for the same scenarios. In the case of S_3 , initially $\bar{k}_a \approx 0.4$ when strong MHD activity is present first in the form of TAEs (from 0.1 to 0.17 s), followed by FBs (from 0.17 to 0.24 s) which are followed by the LLM up to 0.3 s. For $t > 0.3$ s, the perturbation is reduced in amplitude and correspondingly the scaling factor \bar{k}_a tends towards the values of k observed for quiescent scenarios, i.e. $\bar{k}_a \approx 0.6$. In the S_4 case instead, as the MHD activity persists throughout the entire pulse, \bar{k}_a remains suppressed at a level of approximately 0.4. When the scaling factor \bar{k}_a is evaluated for individual impact parameters, times and plasma discharges, the effect of the fast ion redistribution results in a discrepancy between 50 and 70 % with a different scaling than the one

for the quiescent scenarios.

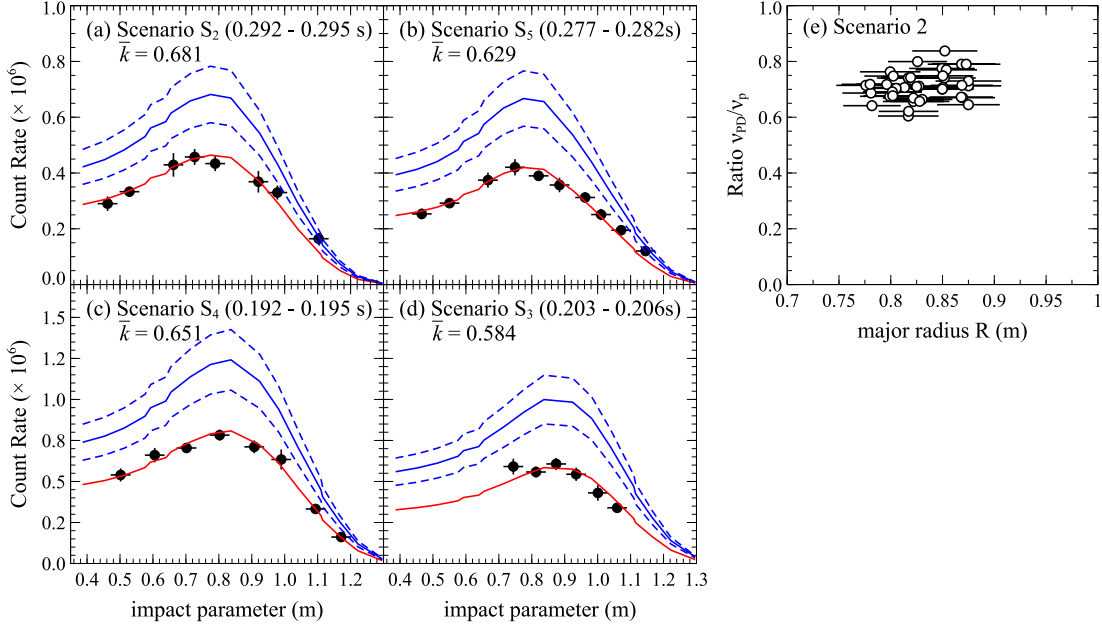


Figure 7 – Panels (a) to (d): comparison between measured (solid circles) and predicted (continuous lines) neutron camera count rates for scenario S_2 to S_5 ; predicted count rates ν_n (solid blue line) are shown with their uncertainties (dashed blue lines) and multiplied by the averaged scaling factor \bar{k} (red lines). Panel (e): ratios between the CFPD count rates ν_{PD} measured by two channels to those predicted by TRANSP ν_p for the plasma discharges of scenario S_2 .

The neutron emission for the representative plasma discharges for scenarios S_2 to S_5 was then recalculated introducing a non-zero, time dependent, anomalous diffusion coefficient in the TRANSP/NUBEAM simulations. For S_3 and S_5 , the FB loss model present in NUBEAM was also used in order to reproduce correctly the sharp drops in the neutron yield at the onset of and during the chirping down phase of these instabilities. The level and time dependence of the anomalous diffusion was obtained by adjusting D_a so that $Y_n(t) \simeq 0.9 \times Y_{FC}(t)$ rather than trying to match $\nu_n(p, t)$ with $\nu_{NC}(p, t)$. This was done for two reasons. The first reason is due to the fact that a manual iterative approach was used to adjust D_a : agreement between measured and predicted neutron yield could be achieved fairly quickly as the number of Monte Carlo particle required is quite small. The second, and most important motivation, is that matching $\nu_n(p, t)$ with $\nu_{NC}(p, t)$ would have required D_a values uncommonly higher than those observed in NSTX ($1 - 2 \text{ m}^2\text{s}^{-1}$) [25, 26] and ASDEX-U (about $1 \text{ m}^2\text{s}^{-1}$) [27] in the presence of similar MHD activity. Good agreement between Y_n and Y_{FC} is obtained with D_a varying between 0 and $2.8 \text{ m}^2\text{s}^{-1}$. With the condition $Y_n(t) \simeq 0.9 \times Y_{FC}(t)$ achieved, new simulations were carried out with large numbers of Monte Carlo particles and the non-flux averaged neutron emissivity was calculated at selected times. Panels (a) to (d) of figure 7 show the comparison between ν_n and ν_{NC} for selected times for scenarios S_2 to S_5 . As can be seen, in all four cases the count rates profiles agree both in shape and amplitude with a scaling factor \bar{k} ranging from 0.58 to 0.68, that is very similar to the case of the quiescent scenarios. The case of scenario S_5 is of particular interest because it confirms that this discrepancy has been present at the same level well before the plasma discharges for the other scenarios were carried out. The same high statistic simulation used for the neutron measurements analysis for scenario S_2 was then used to calculate the ratio ν_{PD}/ν_p which is shown in panel(e) of figure 7 resulting in an average scaling factor $k = 0.71 \pm 0.01$ thus confirming the presence of a deficit in both channels of the DD fusion reaction.

5. Discussion

As shown in the previous section, the deficit between predicted and observed count rates is consistently between 0 and 50 % for both fusion products alike (neutrons and protons) for all different scenarios with and without fast ion redistribution. These observations are summarized in table 3 and in figure 8 for both quiescent and non-quiescent scenarios (when the anomalous fast ion diffusion is included in the TRANSP/NUBEAM modelling).

Scenario	k_{NC}	k_{PD}
S1	0.66 ± 0.01	0.72 ± 0.02
S2	0.68 ± 0.01	0.71 ± 0.01
S3	0.62 ± 0.01	-
S4	0.68 ± 0.01	-
S5	0.63 ± 0.01	-
S6 (pre)	0.63 ± 0.01	0.57 ± 0.01
S6 (post)	0.63 ± 0.01	0.56 ± 0.02

Table 3 – Best estimate of the scaling factor for each scenario from neutron camera data (k_{NC}) and the CFPD (k_{PD}). The labels “pre” and “post” refers to the time intervals before and after a sawtooth crash. The horizontal dash “-” indicates that CFPD measurements are not available.

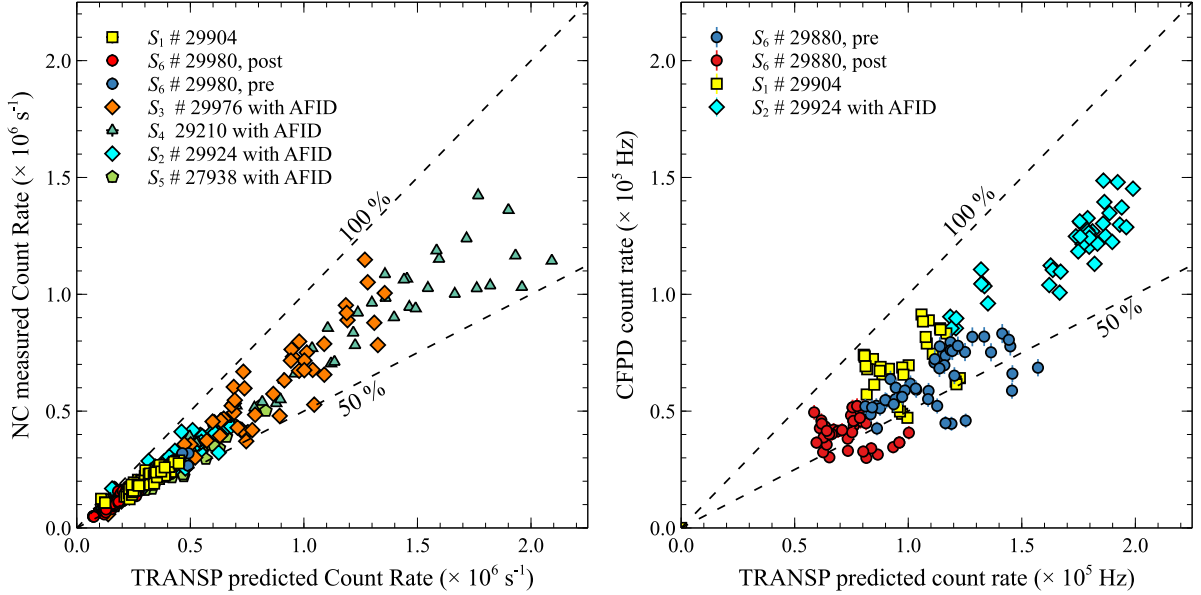


Figure 8 – Comparison between measured count rates by the neutron camera (left panel) and the charged fusion product detector (right panel). For scenarios S_2 to S_5 characterised by strong TAE, FB and LLM activity, TRANSP predictions have been carried out by adjusting the anomalous fast ion diffusion coefficient D_a to match the FC measurements. Each data point represent the ratio between individual NC channels and the TRANSP predicted CRs for selected times during the plasma discharge. The labels “pre” and “post” refers to the time intervals before and after a sawtooth crash.

The observed count rates for the NC and the CFPD are difficult to reconcile with the measurement of the total neutron yield from the fission chamber, even in the simplest quiescent scenarios. Since the same TRANSP/NUBEAM simulation is used to estimate ν_n , ν_p and Y_n it is difficult to understand how the situation in which $Y_n = 0.9Y_{\text{FC}}$ and simultaneously $\nu_{\text{NC}}/\nu_n \approx \nu_{\text{PD}}/\nu_p \approx 0.6$ can arise. One

possibility is that both the NC and CFPD efficiencies are wrongly estimated in such a way that results in a similar ratio between predictions and measurements. Considering that the NC and CFPD are two totally independent diagnostics, relying on completely different physical principles, this seems implausible although it can not be ruled out. An alternative explanation could be that the neutron emissivity used as the starting point for estimating the expected count rates for both the NC and CFPD is incorrect. However, as discussed in section 3.1, the neutron emissivity calculated by TRANSP/NUBEAM agrees very well with the one calculated by DRESS starting from the same underlying fast ion distribution function. In addition, if the neutron emissivity was to be wrong then it would be impossible for the FC to match the TRANSP/NUBEAM predictions for the total neutron yield.

An entirely different explanation for the disagreement between FC and the fusion product measurements is to assume that the original calibration of the fission chamber and its subsequent tracking via activation foils has become unreliable. A close scrutiny of the absolute calibration described in [18] identified few issues that might contribute to this. The first is the lack of the absolute calibration of the ^{252}Cf source which, as stated by the authors of the calibration study, has been calibrated only once 20 years before, using a method known to be accurate to about 2 %. The calibration of the FC on MAST was then performed correcting for the decay of the source using the published half-life of the isotope and assuming the same 2 % uncertainty in the result as obtained for the original calibration. It is noted that a single point calibration of a ^{252}Cf source is not sufficient to determine its isotopic composition and therefore the proportion of the isotope ^{250}Cf was not known at the time of the original source calibration. An isotopic composition different to that assumed might alter the strength of the neutron source, especially as it ages [28], and thus represents an additional, unquantified uncertainty in source strength. A second source of uncertainty in the FC calibration concerns the relative simplicity of the MCNP model used to translate the ^{252}Cf neutron emission to the counts on the fission chamber. The accuracy of the MCNP calculation depends on the detail of the model and the time available for running the code. The model used omitted some details such as the wooden floor around the top of the machine, vessel ports and coil supports leading to an estimate of the error in the MCNP calculation of 8% arising from the combination of the model setup and the Monte-Carlo statistics. When comparing the MCNP results to the ^{252}Cf measurements, the counts predicted were larger than those observed in the FC by a factor of between 24 and 33 with the difference in the scaling factors being dependent on the toroidal position of the ^{252}Cf source. The magnitude of the scaling factors was ascribed to a high acquisition threshold in the electronics attached to the FC and could therefore be normalised using an average factor of 27. However the position dependent variation in the scaling factors (in the range $\pm 17\%$) does not appear to be completely explained by the aforementioned contributions to the total uncertainties in the measurements and modelling. It is also recognised that significant changes to MAST have occurred since this original calibration, most notably the installation of the divertor structure, that have most likely altered the neutron yield. Finally, the cross-calibration with the activation foil is only indicative as the neutron flux on and the activation of the indium foil was not simulated in MCNP. It is also recognised that one of the principal purposes of the FC measurement is to track the total neutron dose in the shielded machine area for safety purposes, particularly tracking activation of machine components to ensure this is below allowed limits. Total neutron dose was assessed after each experimental campaign and in each case, it was found that the dose measured by the FC was higher than that averaged between 12 CR39 neutron monitor badges in the shielded area. It was concluded that although the FC measurement was in disagreement with the badge measurements, operations could safely continue without requiring a re-calibration of the FC. The absolute calibration of a fission chamber on a tokamak is a very complicated endeavour as the recent calibration in JET has highlighted [2]. The points above suggest additional sources of uncertainty in the MAST FC absolute calibration.

Unfortunately, even leaving aside the comparison with the FC measurements, the experimental observations presented in this work indicate that one or multiple systematic error(s) are present in either the NC and CFPD diagnostics or in the TRANSP/NUBEAM inputs and modelling. In section 4.1 it was shown that it is possible to remove the discrepancy by changing, one at the time, the plasma parameters that affect the neutron emissivity such as the effective charge, the electron temperature, the NBI energy and density. However, the required changes are much larger than the accepted uncertainties in these quantities which are therefore discounted as the source of the observed discrepancy. Even envisaging

a situation in which Z_{eff} , T_e , E_{NBI} and n_{NBI} are changed simultaneously within their experimental uncertainty and in the right direction so that predicted and measured count rates agree would not be sufficient to resolve the observed discrepancy. In particular, the NBI energy has been confirmed by measurements of the Doppler shift of the Fast Ions D- α (FIDA) emission. Regarding the absolute intensity of the FIDA signal, related to the NBI intensity, some uncertainties remain which will require further investigation: these will be addressed in a future work. In particular, the role of the halo neutrals during NBI heating has a significant impact on the intensity of both FIDA and NPA signals [29] and was not included in the original FIDA/FIDASim benchmarking [24]. The stored plasma kinetic energy W is an additional plasma parameter that is typically used to check the quality of TRANSP/NUBEAM simulations. On MAST, W is strongly dependent on the NBI heating which contributes to approximately 35 % of its total value [30] and therefore can provide an additional check on the calculated neutron emissivity. Unfortunately on MAST, the diamagnetic loop that is typically used to measure the stored energy was not available for this study.

Losses of fast ions due to charge-exchange processes have been investigated in TRANSP/NUBEAM by modifying both the edge neutral deuterium flux and the external neutral deuterium density $n_{0,\text{ext}}$. In both cases, these quantities have been increased by one order of magnitude with respect to their reference values and no significant difference in the neutron yield was observed. For example, on MAST a fast pressure gauge provides an indication of the neutral molecular deuterium density which, for the plasma scenarios here studied, varied in the range $1 \times 10^{18} - 1 \times 10^{19} \text{ m}^{-3}$ depending on the level of gas puff but no change in the neutron yield was observed when setting $n_{0,\text{ext}} = 1 \times 10^{20} \text{ m}^{-3}$. It is possible that even higher values of $n_{0,\text{ext}}$ might result in a reduction in Y_n but such high density for the neutral D gas are unlikely, especially near the last closed flux surface where most of the charge exchange processes between confined fast ions and neutral atoms and molecules would occur. For example, in NSTX, the atomic and molecular deuterium density have been estimated to be less than 1×10^{17} and $1 \times 10^{18} \text{ m}^{-3}$ with both approaching the atomic density level close to the plasma boundary [31]. On START a very high neutral density was estimated (approximately $1 \times 10^{19} \text{ m}^{-3}$) and was considered as a consequence of the very small ratio between the plasma and the vessel volume (about 7 %) [32]: for comparison the same ratio for NSTX is approximately 50 % and about 20 % on MAST.

Finally, the role of Toroidal Field Ripples (TFRs) on the loss of fast ions in MAST is briefly reviewed here. In a first study, in which a full orbit particle tracking code was used, it was found that TFRs have a negligible impact on the fast ion confinement [33]. However, a more recent study, specifically devoted to the neutron emission modelling along a fast ion trajectory using a non-steady state full orbit following code, suggested that TFRs have a significant role in reducing the confinement of fast ions [6, 7]. In particular, this study suggests a possible explanation for the discrepancy between measured and TRANSP/NUBEAM predicted neutron count rates. In NUBEAM fast ions orbits are calculated using the guiding-centre approximation combined with a finite Larmor radius corrections algorithm to account for the significant size of the Larmor radii of fast ions in MAST compared with the plasma volume and the scale of the spatial gradients of the plasma profiles. Even with this finite Larmor radius correction in place however, the DD fusion reactivity is larger than that calculated when a full orbit following code is used instead [6, 7]. The reason for this is that the size of the fast ion orbits is not negligible compared to the variation in the thermal deuterium density profile. According to this work, the reduction in the neutron yield between guiding-centre (NUBEAM) and full orbit estimates is approximately 30 % giving a ratio of approximately of 0.7 not far from the discrepancy here reported.

6. Conclusions

Neutrons and protons in MAST NBI heated plasmas are produced mainly by the beam-thermal reactions (≈ 90 %) and to a smaller extent to beam-beam reactions (≈ 10 %) with a negligible contribution from thermal fuel reactions. The fusion product deficit reported in this work is independent of the MAST plasma scenario and approximately of the order of 40 %. This discrepancy can not be explained by the uncertainties in the input data to TRANSP/NUBEAM codes unless a large systematic error in one or more such parameters has so far gone undetected. This seems rather unlikely as MAST diagnostics and NBI systems have been well calibrated and validated. The only exception is the fission chamber whose absolute

calibration might have changed in time leading to a coincidental agreement with TRANSP/NUBEAM predictions of the total neutron rate. It might still be the case that systematic errors are present both in the NC and CFPD but the fact that the two independent diagnostics observe a similar deficit in the fusion products from the two different channels of the DD reaction makes this quite unlikely. The fact that both the NC and CFPD synthetic diagnostics use the same neutron emissivity profile to estimate the predicted count rates hints to the possibility of its systematic overestimate by TRANSP/NUBEAM. However, the neutron emissivity profile calculated by TRANSP/NUBEAM and by DRESS agree within 1 % suggesting that the actual quantity that is overestimated is the fast ion density. FIDA diagnostic measurements of the total fast ion density in MAST agree with TRANSP/NUBEAM estimates. However, uncertainties in the absolute calibration of the FIDA diagnostic can not rule out that this agreement is fortuitous especially considering the lack of proper modelling in TRANSP/NUBEAM of the role of the halo neutrals. Assuming that NC and CFPD measurements are correct, the only possible source of the discrepancy that we have identified in this work is the guiding centre approximation used in NUBEAM that was shown to lead to an overestimate of the local neutron emissivity compared to the one calculated by a full orbit following code. This effect is very important in spherical tokamaks due to the large Larmor radius of fast ion orbits compared with the plasma dimensions and the thermal fuel density profile gradients. This might explain why on MAST the fusion product deficit is scenario independent contrary to what is observed on JET, where other factors might be at play. Instead, on conventional tokamaks, with much stronger magnetic fields, the guiding centre approximation might be sufficiently good for neutron rate predictions and measurements to agree, although a careful choice of the effective charge is required [34]. The results and discussion here presented are far from conclusive and further work is needed to better understand and explain the discrepancy between not only fusion product predictions and measurements but also between the NC and CFPD observations with those of the FC and FIDA diagnostics. In particular, the modelling of the fusion product diagnostics using a full orbit following code such as LOCUST-GPU [35] would help to settle the issue: this will be the subject of a follow-up investigation.

Acknowledgments

This work was funded by the Swedish Research Council, the RCUK Energy Programme under grant EP/I501045, the European Union's Horizon 2020 research and innovation programme under grant agreement number 633053 and the U.S. Department of Energy Contract number DE-SC0001157. The views and opinions expressed herein do not necessarily reflect those of the European Commission. The authors are grateful to O. Jones and C. Michael for discussion on the MAST FIDA diagnostic, to M. Fitzgerald and R. Akers for their help with TRANSP/NUBEAM modelling and to K. G. McClements for fruitful discussions on the role of toroidal field ripples and guiding-centre approximations.

References

- [1] Weisen H, Kim H T, Strachan J, Scott S, Baranov Y, Buchanan J, Fitzgerald M, Keeling D, King D, Giacomelli L, Koskela T, Weisen M, Giroud C, Maslov M, Core W, Zastrow K D, Syme D, Popovichev S, Conroy S, Lengar I, Snoj L, Batistoni P, Santala M and Contributors J 2017 *Nuclear Fusion* **57** 076029 URL <http://stacks.iop.org/0029-5515/57/i=7/a=076029>
- [2] Syme D, Popovichev S, Conroy S, Lengar I, Snoj L, Sowden C, Giacomelli L, Hermon G, Allan P, Macheta P, Plummer D, Stephens J, Batistoni P, Prokopowicz R, Jednorog S, Abhangi M and Makwana R 2014 *Fusion Engineering and Design* **89** 2766 – 2775 ISSN 0920-3796 URL <http://www.sciencedirect.com/science/article/pii/S0920379614005274>
- [3] Goldston R J *et al.* 1981 *J. Comput. Phys* **43** 61
- [4] Pankin A, McCune D, Andre R, Bateman G and Kritiz A 2004 *Commun. Comput. Phys.* **159** 157
- [5] Darke A C *et al.* 1995 *MAST: a Mega Amp Spherical Tokamak* (Proc. 18th Symp. on Fusion Technology (Karlsruhe, Germany, 2226 August 1994) vol 1 (Amsterdam: Elsevier) p 799)
- [6] Tani K, Shinohara K, Oikawa T, Tsutsui H, McClements K G, Akers R J, Liu Y Q, Suzuki M, Ide S, Kusama Y and Tsuji-Iio S 2016 *Plasma Physics and Controlled Fusion* **58** 105005 URL <http://stacks.iop.org/0741-3335/58/i=10/a=105005>
- [7] McClements K, Tani K, Akers R J, Liu Y Q, Shinohara K, Tsutsui H and Tsuji-Iio S 2018 *Submitted to Plasma Physics and Controlled Fusion* URL arxiv.org/abs/1806.05940
- [8] Cecconello M, Jones O M, Boegl W U, Perez R V, Darrow D S, Klimek I, Sharapov S E, Fitzgerald M, McClements K G, Keeling D L, Allan S Y, Michael C A, Akers R J, Conway N J, Scannell R,

- Turnyanskiy M, Ericsson G and the MAST Team 2015 *Plasma Physics and Controlled Fusion* **57** 014006 URL <http://stacks.iop.org/0741-3335/57/i=1/a=014006>
- [9] Cecconello M, Sangaroon S, Conroy S, Donato M, Ericsson G, Marini-Bettolo C, Ronchi R, Strom P, Weiszflog M, Wodniak I, Turnyanskiy M, Akers R, Cullen A, Fitzgerald I, McArdle G, Pacoto C and Thomas-Davies N 2014 *Nuclear Instruments and Methods in Physics Research Section A: Accelerators, Spectrometers, Detectors and Associated Equipment* **753** 72 – 83 ISSN 0168-9002 URL <http://www.sciencedirect.com/science/article/pii/S0168900214003702>
 - [10] Perez R V, Boeglin W U, Darrow D S, Cecconello M, Klimek I, Allan S Y, Akers R J, Keeling D L, McClements K G, Scannell R, Turnyanskiy M, Angulo A, Avila P, Leon O, Lopez C, Jones O M, Conway N J and Michael C A 2014 *Review of Scientific Instruments* **85** 11D701 (Preprint <https://doi.org/10.1063/1.4889736>) URL <https://doi.org/10.1063/1.4889736>
 - [11] Goorley T, James M, Booth T, Brown F, Bull J, Cox L J, Durkee J, Elson J, Fensin M, Forster R A, Hendricks J, Hughes H G, Johns R, Kiedrowski B, Martz R, Mashnik S, McKinney G, Pelowitz D, Prael R, Sweezy J, Waters L, Wilcox T and Zukaitis T 2012 *Nuclear Technology* **180** 298–315 (Preprint <https://doi.org/10.13182/NT11-135>) URL <https://doi.org/10.13182/NT11-135>
 - [12] Klein H and Neumann S 2002 *Nuclear Instruments and Methods in Physics Research Section A: Accelerators, Spectrometers, Detectors and Associated Equipment* **476** 132 – 142 ISSN 0168-9002 int. Workshop on Neutron Field Spectrometry in Science, Technology and Radiation Protection URL <http://www.sciencedirect.com/science/article/pii/S0168900201014103>
 - [13] Bähr C, Böttger R, Klein H, von Neumann-Cosel P, Richter A, Schmidt D, Schweda K and Strauch S 1998 *Nuclear Instruments and Methods in Physics Research Section A: Accelerators, Spectrometers, Detectors and Associated Equipment* **411** 430 – 436 ISSN 0168-9002 URL <http://www.sciencedirect.com/science/article/pii/S0168900298004288>
 - [14] Schweda K and Schmidt D 2002 *Nuclear Instruments and Methods in Physics Research Section A: Accelerators, Spectrometers, Detectors and Associated Equipment* **476** 155 – 159 ISSN 0168-9002 int. Workshop on Neutron Field Spectrometry in Science, Technology and Radiation Protection URL <http://www.sciencedirect.com/science/article/pii/S016890020101422X>
 - [15] Weber C, Fabry I, Huhn V, Siepe A and von Witsch W 2002 *Nuclear Instruments and Methods in Physics Research Section A: Accelerators, Spectrometers, Detectors and Associated Equipment* **488** 307 – 313 ISSN 0168-9002 URL <http://www.sciencedirect.com/science/article/pii/S0168900202004321>
 - [16] Dietze G and Klein H 1982 *Technical Report, Physikalisch-Technische Bundesanstalt Braunschweig, PTB-ND-22, Germany*
 - [17] Lao L, Ferron J, Groebner R, Howl W, John H S, Strait E and Taylor T 1990 *Nuclear Fusion* **30** 1035 URL <http://stacks.iop.org/0029-5515/30/i=6/a=006>
 - [18] Stammers K and Loughlin M 2006 *Nuclear Instruments and Methods in Physics Research Section A: Accelerators, Spectrometers, Detectors and Associated Equipment* **562** 521 – 530 ISSN 0168-9002 URL <http://www.sciencedirect.com/science/article/pii/S0168900206004955>
 - [19] Klimek I, Cecconello M, Gorelenkova M, Keeling D, Meakins A, Jones O, Akers R, Lupelli I, Turnyanskiy M, Ericsson G and the MAST Team 2015 *Nuclear Fusion* **55** 023003 URL <http://stacks.iop.org/0029-5515/55/i=2/a=023003>
 - [20] Eriksson J, Conroy S, Sundn E A and Hellesen C 2016 *Computer Physics Communications* **199** 40 – 46 ISSN 0010-4655 URL <http://www.sciencedirect.com/science/article/pii/S0010465515003902>
 - [21] Bosch H S and Hale G 1992 *Nuclear Fusion* **32** 611 URL <http://stacks.iop.org/0029-5515/32/i=4/a=I07>
 - [22] Scannell R, Walsh M J, Carolan P G, Darke A C, Dunstan M R, Huxford R B, McArdle G, Morgan D, Naylor G, OGorman T, Shibaev S, Barratt N, Gibson K J, Tallents G J and Wilson H R 2008 *Review of Scientific Instruments* **79** 10E730 (Preprint <https://doi.org/10.1063/1.2971971>) URL <https://doi.org/10.1063/1.2971971>
 - [23] Patel A, Carolan P G, Conway N J and Akers R J 2004 *Review of Scientific Instruments* **75** 4944–4950 (Preprint <https://doi.org/10.1063/1.1808915>) URL <https://doi.org/10.1063/1.1808915>
 - [24] Michael C A, Conway N, Crowley B, Jones O, Heidbrink W W, Pinches S, Braeken E, Akers R, Challis C, Turnyanskiy M, Patel A, Muir D, Gaffka R and Bailey S 2013 *Plasma Physics and Controlled Fusion* **55** 095007 URL <http://stacks.iop.org/0741-3335/55/i=9/a=095007>
 - [25] Heidbrink W, Ruskov E, Liu D, Stagner L, Fredrickson E, Podestà M and Bortolon A 2016 *Nuclear Fusion* **56** 056005 URL <http://stacks.iop.org/0029-5515/56/i=5/a=056005>
 - [26] Podestà M, Gorelenkova M, Darrow D, Fredrickson E, Gerhardt S and White R 2015 *Nuclear Fusion* **55** 053018 URL <http://stacks.iop.org/0029-5515/55/i=5/a=053018>
 - [27] Zeeland M A V, Heidbrink W W, Fisher R K, Muoz M G, Kramer G J, Pace D C, White R B, Aekaslopolo S, Austin M E, Boom J E, Classen I G J, da Graa S, Geiger B, Gorelenkova M, Gorelenkov N N, Hyatt A W, Luhmann N, Maraschek M, McKee G R, Moyer R A, Muscatello C M, Nazikian R, Park H, Sharapov S, Suttrop W, Tardini G, Tobias B J, Zhu Y B, DIII-D and Teams A U 2011 *Physics of Plasmas* **18** 056114 (Preprint <https://doi.org/10.1063/1.3574663>) URL <https://doi.org/10.1063/1.3574663>
 - [28] A L Roquemore D S D and Medley S S Absolute calibration of the nstx neutron monitor system *24th Symposium on Fusion Engineering* (Chicago, IL)
 - [29] Medley S S, Liu D, Gorelenkova M V, Heidbrink W W and Stagner L 2016 *Plasma Physics and Controlled Fusion* **58** 025007 URL <http://stacks.iop.org/0741-3335/58/i=2/a=025007>
 - [30] Akers R J, Ahn J W, Antar G Y, Appel L C, Applegate D, Brickley C, Bunting C, Carolan P G, Challis C D, Conway N J, Counsell G F, Dendy R O, Dudson B, Field A R, Kirk A, Lloyd B, Meyer H F, Morris A W, Patel A, Roach C M, Rohzansky V, Sykes A, Taylor D, Tournianski M R, Valovic M, Wilson H R, Axon K B, Buttery R J, Ciric D, Cunningham G, Dowling J, Dunstan M R, Gee S J, Gryaznevich M P, Helander P, Keeling D L, Knight P J, Lott F, Loughlin M J, Manhood S J, Martin R, McArdle G J, Price M N, Stammers

- K, Storrs J, Walsh M J, the MAST and Team N 2003 *Plasma Physics and Controlled Fusion* **45** A175 URL <http://stacks.iop.org/0741-3335/45/i=12A/a=013>
- [31] Stotler D P, Scotti F, Bell R E, Diallo A, LeBlanc B P, Podest M, Roquemore A L and Ross P W 2015 *Physics of Plasmas* **22** 082506 (*Preprint* <https://doi.org/10.1063/1.4928372>) URL <https://doi.org/10.1063/1.4928372>
- [32] Akers R, Appel L, Carolan P, Conway N, Counsell G, Cox M, Gee S, Gryaznevich M, Martin R, Morris A, Nightingale M, Sykes A, Mironov M and Walsh M 2002 *Nuclear Fusion* **42** 122 URL <http://stacks.iop.org/0029-5515/42/i=2/a=302>
- [33] McClements K G and Hole M J 2012 *Physics of Plasmas* **19** 072514 (*Preprint* <https://doi.org/10.1063/1.4737605>) URL <https://doi.org/10.1063/1.4737605>
- [34] Tardini G, Hhbauer C, Fischer R, Neu R and the ASDEX Upgrade Team 2013 *Nuclear Fusion* **53** 063027 URL <http://stacks.iop.org/0029-5515/53/i=6/a=063027>
- [35] Akers R J, Verwichte E, Martin T J, Pinches S D and Lake R 2012 Gpgpu monte carlo calculation of gyro-phase resolved fast ion and n-state resolved neutral deuterium distributions *9th EPS Conference on Plasma Physics 16th International Congress on Plasma Physics 2 - 6 July 2012* (Stockholm) p P5.088 URL ocs.ciemat.es/epsicpp2012pap/pdf/P5.088.pdf